V24 Controller Design Using Incremental Nonlinear Dynamic Inversion

Autoflight Flight Control Team

May 19, 2019

Contents

Nomenclature

α	Angle of attack [radian]
$\bar{c}$	Mean aerodynamic chord of the wing $[m]$
$\bar{q}$	Dynamic pressure $[kg/m/s^2]$
β	Angle of sideslip [radian]
$\mathbf{0}$	Zero vector
$\boldsymbol{\mathcal{R}}_a^b$	Rotation matrix or coordinate transformtion matrix from frame a to frame b
$\boldsymbol{\Omega}$	Angular velocity of airframe $[radian/s]$
$\boldsymbol{\omega}_i$	Angular velocity of the i^{th} lifting rotor $[radian/s]$
$\boldsymbol{\omega}_p$	Angular velocity of the pusher propeller $[radian/s]$
$\boldsymbol{\tau}_i$	Torque generated by the i^{th} propeller, $i = 1, 2, 3, ..., 7$ $[N \cdot m]$
$\boldsymbol{F_A}$	Fixed-wing aerodynamic force
$\boldsymbol{f}_i$	Force generated by the i^{th} propeller, $i = 1, 2, 3, ..., 7$ $[N]$
$\boldsymbol{I}_p$	Moment of inertia matrix of the pusher propeller $[kg \cdot m^2]$
$\boldsymbol{I}_r$	Moment of intertia matrix one lifting rotor $[kg \cdot m^2]$
$\boldsymbol{I}_v$	Moment of intertia matrix of the vehicle $[kg \cdot m^2]$
$\boldsymbol{I}_{n\times n}$	Identity matrix with dimension n
$\boldsymbol{M_f}$	Moment associated with fixed-wing aerodynamics $[N \cdot m]$
$\boldsymbol{M_p}$	Moment vector acting on the pusher propeller $[N \cdot m]$
$\boldsymbol{M_r}$	Moment generated by lifting rotors and the pusher propeller $[N \cdot m]$
$\boldsymbol{M_v}$	Resultant moment acting on the vehicle $[N \cdot m]$
$\boldsymbol{M_{rc}}$	Control moments generated by lifts and rotational air drag
$\boldsymbol{M_{rg}}$	Gyroscopic effect of the rotors and pusher
$\boldsymbol{V}$	True air velocity $[m/s]$
$\boldsymbol{v}_i$	Velocity of the i^{th} motor relative to air

δ_a^i, δ_a^o	Angle of aileron deflection [°]
$\delta_e^c, \delta_e^i, \delta_e^o$	Angle of elevator deflection [°]
δ_r	Angle of rudder deflection [°]
ρ	Air density $[kg/m^3]$
b	Wing span $[m]$
C_L, C_D	Nondimensional coefficients of lift and drag
C_l, C_m, C_n	Nondimensional coefficients of roll, pitch and yaw aerodynamic moments
C_X, C_Y, C_Z	Nondimensional coefficients of aerodynamic force in body frame
h	Flight altitude
$O_{\mathcal{B}}$	NED frame with axes Ox, Oy and Oz
$O_{\mathcal{I}}$	NED frame with axes Ox_N, Ox_E and Ox_D
O_g	Geometric frame with axes Ox_g, Oy_g and Oz_g
p, q, r	Angular velocity of airframe resolved in body frame along X, Y and Z axis $[radian/s]$
S	Wing reference area $[m^2]$
u	Control inputs
$V_x^{\mathcal{B}}, V_y^{\mathcal{B}}, V_z^{\mathcal{B}}$	Aircraft velocity resolved in body frame along Ox, Oy and Oz axis $[m/s]$
x	States
X, Y, Z	Aerodynamic force acting on the aircraft along Ox, Oy and Oz axis $[N]$
x_c^g, y_c^g, z_c^g	Position of center of gravity resolved in geometric frame
$\boldsymbol{M}_{\boldsymbol{r}i}$	Moment vector acting on the i^{th} lifting rotors $[N \cdot m]$

Chapter 1

Mathematical Model of V24

1.1 Reference Frames and Sign Convention

Clear and resonable choices of reference frames and sign conventions are important for developing mathematical model and controller of an aircraft. Take [1] as a reference, all reference frames and sign conventions that will be used are defined in this section. All reference frames are right handed and with mutually orthogonal axes. Some commonly used notations, reference frames and sign conventions are shown in Figure.1.1.

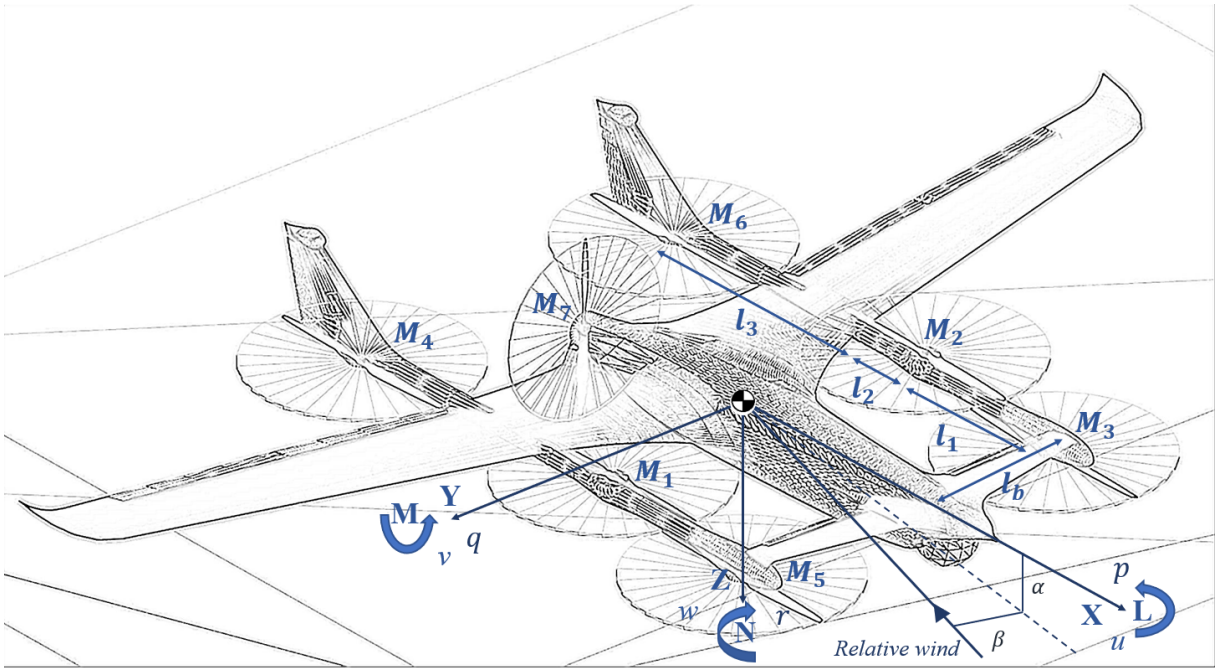

Figure 1.1: V24 VTOL aircraft with body frame definition. X, Y, and Z are body-axis components of aerodynamic force acting on the aircraft; L, M, N are body-axis components of aerodynamic moment acting on the aircraft; p, q, r are body-axis components of aircraft angular velocity; u, v, w are body-axis components of aircraft velocity relative to NED frame.

1.1.1 Reference Frames

NED Frame ($Ox_Ny_Ez_D$ or $O_\mathcal{I}$)

Origin is at an arbitrary point on the sureface of Earth, with positive Ox_N axis pointing toward geographic north, positive Oy_E axis pointing east, and positive Oz_D axis pointing to the center of Earth. It is assumed that the surface of Earth is flat and motion of Earth is neglectful and hence NED frame becomes an inertia frame.

Body Frame ($Oxyz$ or $O_{\mathcal{B}}$)

Origin is at center of gravity of the aircraft, with positive O_x axis pointing forward through the nose of the aircraft, positive O_y axis perpendicular to the geometric plane of symmetry for the aircraft out the right wing, and positive O_z axis is the completion of the right handed coordinate system. Note that the moment of inertia of the aircraft is measured and given with respected to body frame, which is discussed in detail in Appendix A.

Local Frame $Ox_l y_l z_l$

Local frame is obtained by simply translating O_{NED} to the position at which V24 takes off. Therefore it is a frame just as same as O_{NED} but with different origin.

Stability Frame $Ox_s y_s z_s$

Stability frame blablablabla...

Wind Frame ($Ox_w y_w z_w$ or $O_{\mathcal{W}}$)

Origin is at the aircraft *c.g.*, with positive Ox_w axis pointed diretly into the air-relative velocity (true air velocity $\boldsymbol{V}$), positive Oz_w axis remained on the Oxz plane of body frame and rotated so that it is perpendicular to Ox_w axis, and Oy_w axis completed the right-handed system. Lifts and drags are commonly provided in wind frame. The transformation from body to wind axes consists of two rotations. First the body axes are rotated about the y-axis through the angle of attack α; the axes are then rotated about the z-axis through the angle of sideslip β, yielding the wind axes.

Geometric Frame O_g or $Ox_g y_g z_g$

Origin is at the center of rotation of the pusher propeller, with positive Ox_g axis pointing from origin towards the nose of the aircraft, positive Oy_g axis perpendicular to the geometric plane of symmetry for the aircraft out the right wing, and positive O_z axis is the completion of the right handed coordinate system. Under the multiples assumptions made in section 1.2, the three axes of O_g are all respectively coincide with axes of $O_{\mathcal{B}}$, with simply moving origin of $O_{\mathcal{B}}$ from *c.g* to the center of rotation of the pusher propeller.

1.1.2 Sign Conventions

For angular velocities or applied moments, the sign convention follows the right-hand rule. Angular velocities or applied moments about the O_x, O_y, and O_z body axes are described with the adjectives roll, pitch, and yaw, respectively.

As shown in Figure 1.2a, there are totally 8 control surfaces on V24. Although each control surface is able to move independently of the others, fixed-wing aerodynamic models and flight controllers usually treat control surfaces as several groups each of which has some prescribed, specific motions. For V24, the 8 control surfaces are divided into 4 groups, namely, surface 1 and 2, 4 and 5, 3 and 6, and 7 and 8. The group of surface 7 and 8 is only utilized as rudder, which means they always move in the same direction with same defelction angle. All of the

other three groups will function as both elevator and aileron, with sign convention depicted in Figure 1.2b where δ_a is for aileron, δ_e is for elevator and δ_r is for rudder.

Since there are multiple ailerons and elevators, let δ_a^i the aileron deflection angle of surface 4 and 5, and δ_a^o the aileron deflection angle of surface 3 and 6. And let δ_e^i the elevator deflection angle of surface 4 and 5, and δ_e^o the elevator deflection angle of surface 3 and 6. Note that in each group of control surfaces, magnitudes of the upward and downward aileron deflections are the same. The canard will only be used as elevator, so let δ_e^c denote the canard deflection(there is no δ_a^c).

Indexing and directions of rotation of lifting rotors and pusher are shown in Figure 1.2a.

1.2 Mass and Geometric Properties

1.2.1 Geometric Properties

The geometric properties of V24 are shown in Figure 1.3. Note that V24 has a geometrically symmetric plane: O_g-Ox_g-Oz_g. Also notice that, as shown in Figure 1.2a, motor 3,4,5 and 6 point downwards and motor 1 and 2 point upwards. It is assumed that the line jointing motor 1 and 2 is parallel to Ox_g which is also parallel to the plane formed by motor 3,4,5 and 6. Some commonly used geometric properties are listed below (Figure 1.1):

- $l_b = 0.580m$
- $l_1 = 0.575m$
- $l_2 = 0.266m$
- $l_3 = 0.839m$

1.2.2 Center of Gravity

Let x_c^g, y_c^g and z_c^g denote the coordinates of center of gravity resolved in geometric frame O_g. Based on experimental results, $x_c^g = 1.19m$. In design, manufacture and assembling of V24 it is expected that the $c.g.$ is on the plane of geometric symmetry, which in practice is never the case. In the future the true y_c^g will be determined experimentally but for now it is assumed that the distance between $c.g.$ and plane O_g-Ox_g-Oz_g is neglectful, therefore $y_c^g = 0$. Besides, assume that $z_c^g = 0$ so the pusher does not generate any pitching moment.

1.2.3 Moment of Intertia

Assume that the distribution of mass is symmetric with respect to plane O_g-Ox_g-Oz_g, which means that

$$I_v = \begin{bmatrix} I_{v_{xx}} & 0 & I_{v_{xz}} \\ 0 & I_{v_{yy}} & 0 \\ I_{v_{xz}} & 0 & I_{v_{zz}} \end{bmatrix}. \tag{1.1}$$

There are two types of methods in determing moment of inertia of an aircraft: experimental determination and software-based estimation. A detailed discussion can be found in Appendix A. In short, with proper error analysis and correct experimental operation, the first method

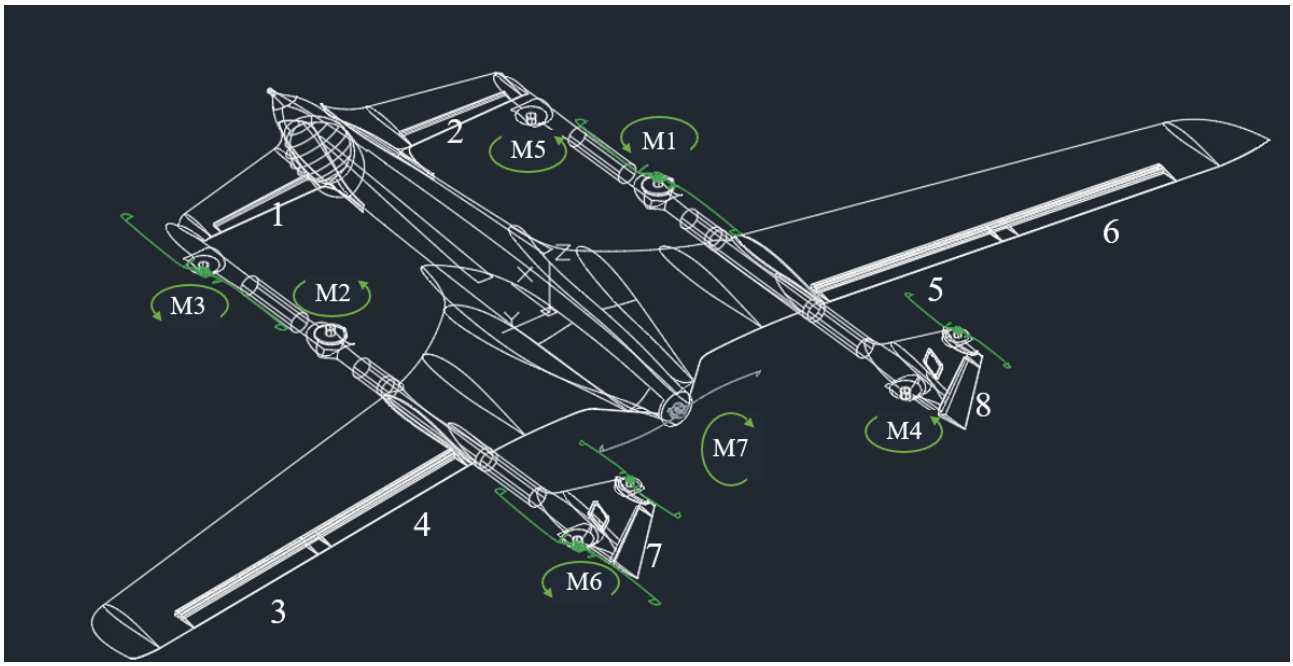

(a) Wing reference area used for V24 (area enclosed by orange lines) and definition of root chord and tip chord.

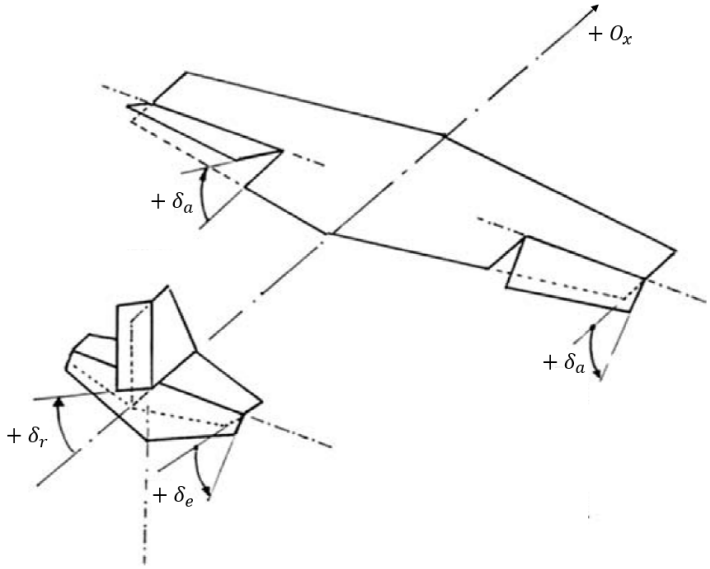

(b) Sign convention of control surfaces.

Figure 1.2: Wing reference area and mean aerodynamic chord.

is able to provide very accurate results, but it is difficult to measure $I_{v_{xz}}$ due to complicated experimental setup and much more sources of error. To the contrary, the second method can give a complete information about moment of inertia, but the result is not as accurate as that of the first method because in practice it is extremely difficult and time-consuming to precisely include every single component of the aircraft, especially wires, the fuselage and screws. For now, only the first method has been applied to determine $I_{v_{xx}}, I_{v_{yy}}$ and $I_{v_{zz}}$, and the results are listed below:

- $I_{v_{xx}} = 10.1154kg \cdot m^2$

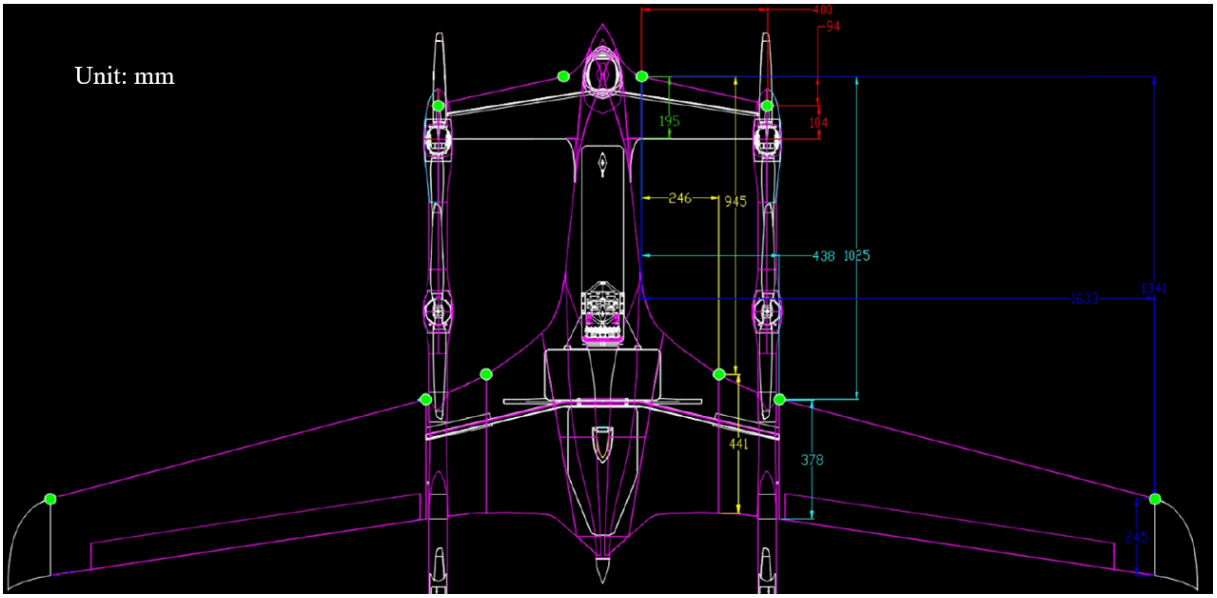

Figure 1.3: Geometric properties of V24. The unit is millimeter.

- $I_{v_{yy}} = 6.9543kg \cdot m^2$
- $I_{v_{zz}} = 10.7149kg \cdot m^2$

1.3 Modeling of Actuators

NOTICE: The content in this section is purely based on literatrue research. In other words, this section presents what we plan to do to model actuators.

1.3.1 ESC & Motor & Propeller

Static Model

The static model relates angular speed of propeller to generated force and moment. According to CFD results and [3], the force generated by a propeller is not only a function of its angular speed, but also of vehicular attitude, velocity and geometric properties. In brief case, let $\boldsymbol{f}_i$ and $\boldsymbol{\tau}_i$ denote the force and aerodynamic drag torque generated by the i^{th} propeller (i is from 1 to 7 where $i = 7$ stands for the pusher: $\boldsymbol{\omega}_7 = \boldsymbol{\omega}_p$, see Figure 1.2a), then

$$\boldsymbol{f}_i = f(\boldsymbol{\Omega}, \boldsymbol{\omega}_i, V_x^{\mathcal{B}}, V_y^{\mathcal{B}}, V_z^{\mathcal{B}}, i) \tag{1.2}$$

where $V_x^{\mathcal{B}}, V_y^{\mathcal{B}}$ and $V_z^{\mathcal{B}}$ are coordinates of $\boldsymbol{V}$ resolved in body($O_{\mathcal{B}}$) frame. Note that the relation changes with different propeller, which is the reason why index of propller, i, is on the right hand side of Eqn.1.2. This variation in static model is due to some specific geometric properties of V24 airframe configuration, e.g., motor 2 and motor 3's disks are partially overlapping with each other, causing changes in propeller air flow and hence changes in force and torque.

The static model can be obtained by theoretical analysis, CFD or experimental determination, while system identification might not be suitable for this purpose. For experimental determination, it is not difficult to get $\boldsymbol{f}_i$ at $\boldsymbol{V} = \boldsymbol{0}$, but for $\boldsymbol{V} \neq \boldsymbol{0}$, wind tunnel tests are required. The current approach is to utilize the first and the second method to obtain the relation as a

database formed by interpolation on a multi-dimensional matrix of specific data points. The experimental results at $\boldsymbol{V} = \mathbf{0}$ are used merely as a validation.

Assume that the effect of $\boldsymbol{\omega}$ on torque and force is only related to $\omega_z^{\mathcal{B}}$, in other words, $\boldsymbol{\omega}$ will be replaced by spinning speed of the motor. Besides, because V24 is symmetric with respect to plane O_{xz}, it is assume that the three motors on the left have the same static model as the three on the right:

$$\begin{aligned} f(\boldsymbol{\Omega}, \boldsymbol{\omega}, V_x^{\mathcal{B}}, V_y^{\mathcal{B}}, V_z^{\mathcal{B}}, 1) &= f(\boldsymbol{\Omega}, \boldsymbol{\omega}, V_x^{\mathcal{B}}, V_y^{\mathcal{B}}, V_z^{\mathcal{B}}, 2) \\ f(\boldsymbol{\Omega}, \boldsymbol{\omega}, V_x^{\mathcal{B}}, V_y^{\mathcal{B}}, V_z^{\mathcal{B}}, 3) &= f(\boldsymbol{\Omega}, \boldsymbol{\omega}, V_x^{\mathcal{B}}, V_y^{\mathcal{B}}, V_z^{\mathcal{B}}, 5) \\ f(\boldsymbol{\Omega}, \boldsymbol{\omega}, V_x^{\mathcal{B}}, V_y^{\mathcal{B}}, V_z^{\mathcal{B}}, 4) &= f(\boldsymbol{\Omega}, \boldsymbol{\omega}, V_x^{\mathcal{B}}, V_y^{\mathcal{B}}, V_z^{\mathcal{B}}, 6) \end{aligned} \tag{1.3}$$

A detailed description of how the static model is calculated and the corresponding results can be found in Appendix B. To detrive the relation f, let $\boldsymbol{r}_i^{\mathcal{B}}$ denote the vector of position of the i^{th} motor relative to $O_{\mathcal{B}}$ resolved in body frame. Hence

$$\boldsymbol{r}_1^{\mathcal{B}} = \begin{bmatrix} l_2 \\ l_b \\ 0 \end{bmatrix} \quad \boldsymbol{r}_2^{\mathcal{B}} = \begin{bmatrix} l_2 \\ -l_b \\ 0 \end{bmatrix} \quad \boldsymbol{r}_3^{\mathcal{B}} = \begin{bmatrix} l_2 + l_1 \\ -l_b \\ 0 \end{bmatrix} \quad \boldsymbol{r}_4^{\mathcal{B}} = \begin{bmatrix} -l_3 \\ l_b \\ 0 \end{bmatrix} \quad \boldsymbol{r}_5^{\mathcal{B}} = \begin{bmatrix} l_2 + l_1 \\ l_b \\ 0 \end{bmatrix} \quad \boldsymbol{r}_6^{\mathcal{B}} = \begin{bmatrix} -l_3 \\ -l_b \\ 0 \end{bmatrix} \tag{1.4}$$

Then based on the assumption made in 1.4, the velocity of the i^{th} motor relative to air is

$$\boldsymbol{v}_i = \boldsymbol{V} + \boldsymbol{r}_i \times \boldsymbol{\Omega} \tag{1.5}$$

Compute Eq.1.5 in body frame:

$$\boldsymbol{v}_i^{\mathcal{B}} = \boldsymbol{\mathcal{R}}_{\mathcal{I}}^{\mathcal{B}} \boldsymbol{V}^{\mathcal{I}} + \boldsymbol{r}_i^{\mathcal{B}} \times \boldsymbol{\Omega}^{\mathcal{B}} \tag{1.6}$$

where $\boldsymbol{\mathcal{R}}_{\mathcal{I}}^{\mathcal{B}}$ is the rotation matrix defined in Sec.1.4.2, $\boldsymbol{V}^{\mathcal{I}}$ is the velocity of V24 in NED frame and $\boldsymbol{\Omega}^{\mathcal{B}} = [p, q, r]^T$. Then assume that the perpendicular velocity relative to air $(V_x^{\mathcal{B}}, V_y^{\mathcal{B}})$ have effects on propeller force and torque that are independent of lateral relative-to-air velocity $(V_z^{\mathcal{B}})$. And the corresponding force and torque each propeller generated can hence be obtained from the CFD database.

Dynamic Model

Let u denote the control input to the ESC. The dynamic model describes the relation between control input u and angular speed of the propeller $|\boldsymbol{\omega}|$(strictly speaking, this only holds when $\boldsymbol{V} = \boldsymbol{\Omega} = \mathbf{0}$). Here the subscript index i is dropped because the influence of motor position on dynamic model is neglectful. In the perspective of control, the system consisting of ESC, brushless motor and propeller is a fully-developed, complicated closed-loop system, which means modeling from the level of circuit and magnet is extremely difficult and time-consuming. Alternatively, [4] provides an approach in which the whole system is considered as a grey box model whose structure is determined by emprical formulas with unknow paramters obtained using system identification. This method is evaluated to be effective and feasible and hence will be employed in the future. Presented below is the structure of the grey box model that is to be identified:

$$\begin{aligned} \dot{\omega} &= K_1 + K_2\omega + K_3\omega^2 + K_4 e_\omega + K_5 \omega_d \\ \dot{e_\omega} &= \omega_d - \omega \end{aligned} \tag{1.7}$$

where ω is angular speed of the propeller, ω_d is the commanded angular speed and e_ω is an aritificial state standing for error between ω and ω_d. Usually ω_d is a nonlinear function of control input u, e.g., a third order polynomial looks like:

$$\omega_d = a_0 + a_1 u + a_2 u^2 + a_3 u^3 \tag{1.8}$$

where a_0, a_1, a_2 and a_3 are parameters obtained by curve fitting algorithms.

1.3.2 Control Surface

1.4 Aircraft Kinematics

The kinematic equations provided in this section are all based on the following assumptions:

- The aircraft is a rigid body with **fixed** mass distribution and constant mass.
- The air is at rest with respect to NED frame. In other words, there is no steady wind, gusts or wind shears.
- The earth is at rest in inetia space and its surface is flat.
- The gravitational field is uniform, which means the aircraft *c.g.* and center of mass are coincide with each other.

The above assumptions, especially the first three, might be dropped in the future. For example, when APU is used, both mass distribution and total mass of the aircraft will change as fuel are consumed in flight.

1.4.1 Rotational Kinematic Equations

Let ϕ, θ and ψ denote the roll, pitch and yaw Euler angles. Then rotational kinematic equation that relate rate of change of the Euler angles to the body angular velocity is shown in Eq 1.9 below

$$\begin{bmatrix} p \\ q \\ r \end{bmatrix} = \begin{bmatrix} 1 & 0 & -\sin\theta \\ 0 & \cos\phi & \sin\phi\cos\theta \\ 0 & -\sin\phi & \cos\phi\cos\theta \end{bmatrix} \begin{bmatrix} \dot{\phi} \\ \dot{\theta} \\ \dot{\psi} \end{bmatrix} \tag{1.9}$$

1.4.2 Navigation Equations

Let x, y, z denote the components of position vector of aircraft *c.g.* with respect to the origin of local frame resolved in local frame. The navigation equations can then be written as

$$\begin{bmatrix} \dot{x} \\ \dot{y} \\ \dot{z} \end{bmatrix} = \underbrace{\begin{bmatrix} 1 & 0 & 0 \\ 0 & \cos\phi & \sin\phi \\ 0 & -\sin\phi & \cos\phi \end{bmatrix} \begin{bmatrix} \cos\theta & 0 & -\sin\theta \\ 0 & 1 & 0 \\ \sin\theta & 0 & \cos\theta \end{bmatrix} \begin{bmatrix} \cos\psi & \sin\psi & 0 \\ -\sin\psi & \cos\psi & 0 \\ 0 & 0 & 1 \end{bmatrix}}_{\boldsymbol{\mathcal{R}}_{\mathcal{B}}^{\mathcal{I}}} \begin{bmatrix} V_x^{\mathcal{B}} \\ V_y^{\mathcal{B}} \\ V_z^{\mathcal{B}} \end{bmatrix} \tag{1.10}$$

where $\boldsymbol{\mathcal{R}}_{\mathcal{B}}^{\mathcal{I}}$ is the rotation matrix or coordinate transformation matrix from body frame to NED frame. It is worth noting that for a rotation matrix $\boldsymbol{\mathcal{R}}$

$$\boldsymbol{\mathcal{R}}^{-1} = \boldsymbol{\mathcal{R}}^T. \tag{1.11}$$

1.5 Aircraft Dynamics

Let $\Omega = [p, q, r]^T$ denote the angular velocity of the airframe resolved in body frame as in Fig.1.1 and $\dot{\Omega}$ its time derivative. If $\boldsymbol{I}_v$ is the moment of inertia of the vehicle, then according to Euler's equation of motion,

$$\boldsymbol{I}_v\dot{\boldsymbol{\Omega}} + \boldsymbol{\Omega} \times \boldsymbol{I}_v\boldsymbol{\Omega} = \boldsymbol{M_v} \tag{1.12}$$

where $\boldsymbol{M_v}$ is the resultant moment vector acting on the vehicle. For V24 it is assumed that the distribution of mass is symmetric about the O-X-Z plane of body frame, which leading to $\boldsymbol{I}_{xy} = \boldsymbol{I}_{yz} = 0$. The inertia matrix then reduces to

$$\boldsymbol{I}_v = \begin{bmatrix} I_x & 0 & -I_{xz} \\ 0 & I_y & 0 \\ -I_{xz} & 0 & I_z \end{bmatrix} \tag{1.13}$$

Hence the scalar form of dynamic equations of airframe as a rigid body are

$$\begin{aligned} \dot{p}I_x - \dot{r}I_{xz} &= M_{vx} - qr(I_z - I_y) + qpI_{xz} \\ \dot{q}I_y &= M_{vy} - pr(I_x - I_z) - (p^2 - r^2)I_{xz} \\ \dot{r}I_z - \dot{p}I_{xz} &= M_{vz} - pq(I_y - I_x) - qrI_{xz} \end{aligned} \tag{1.14}$$

where $\boldsymbol{M}_{\boldsymbol{v}}^{\mathcal{B}} = [M_{vx}, M_{vy}, M_{vz}]^T$ is the resultant moment acting on airframe resolved in body frame. Now partition the moment vector acting on the vehicle into several parts as shown in Eq.1.15

$$\boldsymbol{M_v} = \boldsymbol{M_f} + \boldsymbol{M_r} \tag{1.15}$$

where $\boldsymbol{M_r}$ is the moment generated by lifting rotors and the pusher propeller and $\boldsymbol{M_f}$ contains all the moments associated with fixed-wing aerodynamics.

1.5.1 Rotorcraft Dynamic Model

To compute $\boldsymbol{M_r}$, further partition it into two parts as in Er.1.16[2]

$$\boldsymbol{M_r} = \boldsymbol{M_{rc}} - \boldsymbol{M_{rg}} \tag{1.16}$$

where$\boldsymbol{M_{rc}}$ is the control moments generated by lifts and rotational air drag and $\boldsymbol{M_{rg}}$ is the gyroscopic effect of the rotors and pusher.

First, consider the rotation of lifting rotors and the pusher in body coordinate system:

$$\boldsymbol{I}_r\dot{\boldsymbol{\omega}}_i + \boldsymbol{\Omega} \times \boldsymbol{I}_r\boldsymbol{\omega}_i = \boldsymbol{M_{r}}_i \tag{1.17}$$

$$\boldsymbol{I}_p\dot{\boldsymbol{\omega}}_p + \boldsymbol{\Omega} \times \boldsymbol{I}_p\boldsymbol{\omega}_p = \boldsymbol{M_p} \tag{1.18}$$

where $\boldsymbol{I}_r$ is the moment of inertia matrix of a lifting rotor, $\boldsymbol{I}_p$ is the moment of inertia matrix of the pusher propeller, $\boldsymbol{\omega}_i$ is the angular velocity of the i^{th} lifting rotor, $\boldsymbol{\omega}_p$ is the angular velocity of pusher propeller, $\boldsymbol{M_r}_i$ is the moment vector acting on the i^{th} lifting rotor and $\boldsymbol{M_p}$ is the moment vector acting on the pusher propeller. Based on the structure of V24, under the condition $\boldsymbol{\Omega} = 0$, $\boldsymbol{\omega}_i$ will always have the same or opposite direction as body Z axis, and $\boldsymbol{\omega}_p$ will always have the same or opposite direction as body X axis. Without loss

of generality, assume that if $\boldsymbol{\Omega} = 0$, then $\boldsymbol{\omega}_1, \boldsymbol{\omega}_3, \boldsymbol{\omega}_6$ have the same direction as body $+\boldsymbol{Z}$ axis, while $\boldsymbol{\omega}_2, \boldsymbol{\omega}_4, \boldsymbol{\omega}_5$ have the same direction as $-\boldsymbol{Z}$, and $\boldsymbol{\omega}_p$ has the same direction as $+\boldsymbol{X}$ axis. Besides, given the geometric properties of pusher and lifting propellers, it is reasonable to make the assumption that all propellers are flat on the corresponding rotating plane, and hence $I_{r_{xz}} = I_{r_{yz}} = I_{p_{xz}} = I_{p_{yz}} = 0$. Resolve Eq.1.17 in body-fixed frame:

$$\begin{bmatrix} I_{r_{xx}} & I_{r_{xy}} & 0 \\ I_{r_{xy}} & I_{r_{yy}} & 0 \\ 0 & 0 & I_{r_{zz}} \end{bmatrix} \begin{bmatrix} \dot{\boldsymbol{\omega}}_{ix} \\ \dot{\boldsymbol{\omega}}_{iy} \\ \dot{\boldsymbol{\omega}}_{iz} \end{bmatrix} + \begin{bmatrix} 0 & -r & q \\ r & 0 & -p \\ -q & p & 0 \end{bmatrix} \begin{bmatrix} I_{r_{xx}} & I_{r_{xy}} & 0 \\ I_{r_{xy}} & I_{r_{yy}} & 0 \\ 0 & 0 & I_{r_{zz}} \end{bmatrix} \begin{bmatrix} \boldsymbol{\omega}_{ix} \\ \boldsymbol{\omega}_{iy} \\ \boldsymbol{\omega}_{iz} \end{bmatrix} = \begin{bmatrix} \boldsymbol{Mr}_{ix} \\ \boldsymbol{Mr}_{iy} \\ \boldsymbol{Mr}_{iz} \end{bmatrix}. \tag{1.19}$$

Then expand it into scalar form as below

$$\begin{aligned} I_{r_{xx}}\dot{\boldsymbol{\omega}}_{ix} + I_{r_{xy}}\dot{\boldsymbol{\omega}}_{iy} - r(I_{r_{xy}}\boldsymbol{\omega}_{ix} + I_{r_{yy}}\boldsymbol{\omega}_{iy}) + qI_{r_{zz}}\boldsymbol{\omega}_{iz} &= \boldsymbol{M}_{\boldsymbol{r}ix} \\ I_{r_{xy}}\dot{\boldsymbol{\omega}}_{iy} + I_{r_{xy}}\dot{\boldsymbol{\omega}}_{iy} + r(I_{r_{xx}}\boldsymbol{\omega}_{ix} + I_{r_{xy}}\boldsymbol{\omega}_{iy}) - pI_{r_{zz}}\boldsymbol{\omega}_{iz} &= \boldsymbol{M}_{\boldsymbol{r}iy} \\ I_{r_{zz}}\dot{\boldsymbol{\omega}}_{iz} - q(I_{r_{xx}}\boldsymbol{\omega}_{ix} + I_{r_{xy}}\boldsymbol{\omega}_{iy}) + p(I_{r_{xy}}\boldsymbol{\omega}_{ix} + I_{r_{yy}}\boldsymbol{\omega}_{iy}) &= \boldsymbol{M}_{\boldsymbol{r}iz}. \end{aligned} \tag{1.20}$$

Notice that typically $\boldsymbol{\omega}_{iy} << \boldsymbol{\omega}_{iz}$ and $\boldsymbol{\omega}_{ix} << \boldsymbol{\omega}_{iz}$. So assume that all terms associated with $\boldsymbol{\omega}_{iy}$, $\boldsymbol{\omega}_{ix}$, $\dot{\boldsymbol{\omega}}_{ix}$ and $\dot{\boldsymbol{\omega}}_{iy}$ are negligible. Hence a simplified equation governing the rotational motion of one lifting rotor is given by Eq.1.21

$$\boldsymbol{M}_{\boldsymbol{r}i} = \begin{bmatrix} qI_{r_{zz}}\boldsymbol{\omega}_{iz} \\ -pI_{r_{zz}}\boldsymbol{\omega}_{iz} \\ I_{r_{zz}}\dot{\boldsymbol{\omega}}_{iz} \end{bmatrix} = \begin{bmatrix} \boldsymbol{M}_{\boldsymbol{r}ix} \\ \boldsymbol{M}_{\boldsymbol{r}iy} \\ \boldsymbol{M}_{\boldsymbol{r}iz} \end{bmatrix}. \tag{1.21}$$

Summing up six lifting rotors, we hence obtain

$$\begin{aligned} \sum_{i=1}^{6} \boldsymbol{M}_{\boldsymbol{r}i} &= \sum_{i=1}^{6} (-1)^{i+1} \begin{bmatrix} qI_{r_{zz}}\boldsymbol{\omega}_{iz} \\ -pI_{r_{zz}}\boldsymbol{\omega}_{iz} \\ I_{r_{zz}}\dot{\boldsymbol{\omega}}_{iz} \end{bmatrix} \\ &= \begin{bmatrix} 0 & 0 & 0 & 0 & 0 & 0 \\ 0 & 0 & 0 & 0 & 0 & 0 \\ I_{r_{zz}} & -I_{r_{zz}} & I_{r_{zz}} & -I_{r_{zz}} & -I_{r_{zz}} & I_{r_{zz}} \end{bmatrix} \begin{bmatrix} \dot{\boldsymbol{\omega}}_{1z} \\ \dot{\boldsymbol{\omega}}_{2z} \\ \dot{\boldsymbol{\omega}}_{3z} \\ \dot{\boldsymbol{\omega}}_{4z} \\ \dot{\boldsymbol{\omega}}_{5z} \\ \dot{\boldsymbol{\omega}}_{6z} \end{bmatrix} \\ &+ \begin{bmatrix} qI_{r_{zz}} & -qI_{r_{zz}} & qI_{r_{zz}} & -qI_{r_{zz}} & -qI_{r_{zz}} & qI_{r_{zz}} \\ -pI_{r_{zz}} & pI_{r_{zz}} & -pI_{r_{zz}} & pI_{r_{zz}} & pI_{r_{zz}} & -pI_{r_{zz}} \\ 0 & 0 & 0 & 0 & 0 & 0 \end{bmatrix} \begin{bmatrix} \boldsymbol{\omega}_{1z} \\ \boldsymbol{\omega}_{2z} \\ \boldsymbol{\omega}_{3z} \\ \boldsymbol{\omega}_{4z} \\ \boldsymbol{\omega}_{5z} \\ \boldsymbol{\omega}_{6z} \end{bmatrix} \end{aligned} \tag{1.22}$$

Similarly, under the assumption that $\boldsymbol{\omega}_{py}$, $\boldsymbol{\omega}_{pz}$, $\dot{\boldsymbol{\omega}}_{py}$, $\dot{\boldsymbol{\omega}}_{pz}$ are negligible, the equation that governing the rotational motion of the pusher propeller is shown below as Eq.1.23

$$\boldsymbol{M}_{\boldsymbol{p}} = \begin{bmatrix} I_{p_{xx}}\dot{\boldsymbol{\omega}}_{px} + \tau_p \\ rI_{p_{xx}}\boldsymbol{\omega}_{px} \\ -qI_{p_{xx}}\boldsymbol{\omega}_{px} \end{bmatrix} = \begin{bmatrix} \boldsymbol{M}_{\boldsymbol{p}_x} \\ \boldsymbol{M}_{\boldsymbol{p}_y} \\ \boldsymbol{M}_{\boldsymbol{p}_z} \end{bmatrix}. \tag{1.23}$$

where $\tau_p = |\boldsymbol{\tau}_{\boldsymbol{p}}|$ is the torque on the pusher generated by air drag.

Combining Eq.1.23 and Eq.1.22 together, we obtain

$$\boldsymbol{M_{rg}} = \sum_{i=1}^{6} \boldsymbol{M_{r}}_i + \boldsymbol{M_p} \tag{1.24}$$

Next, based on the sign convention and some simple dynamic laws, the control moments $\boldsymbol{M_{rc}}$ can be expressed as

$$\boldsymbol{M_{rc}} = \begin{bmatrix} l_b(f_2 + f_3 + f_6 - f_1 - f_4 - f_5) \\ (f_1 + f_2)l_2 + (f_3 + f_5)(l_1 + l_2) - (f_4 + f_6)l_3 \\ \tau_1 - \tau_2 + \tau_3 - \tau_4 - \tau_5 + \tau_6 \end{bmatrix} \tag{1.25}$$

where $f_i = |\boldsymbol{f}_i|$ and $\tau_i = |\boldsymbol{\tau}_i|$.

1.5.2 Fixed-wing Aerodynamic Model

Aerodynamic Force

Assume that the aerodynamic forces acting on V24 can be written in the form of

$$\boldsymbol{F_A}\Big|_{\mathcal{B}} = \bar{q}S \begin{bmatrix} C_X \\ C_Y \\ C_Z \end{bmatrix} \tag{1.26}$$

where $\bar{q} = (1/2)\rho|\boldsymbol{V}|^2$ is the dynamic pressure, $|\boldsymbol{V}|$ is the magnitude of the true airspeed, ρ is the air density, S is the wing reference area and C_X, C_Y, C_Z are nondimensional coefficients of aerodynamic force in body frame. If the aerodynamic force is expressed in wind frame, then C_X and C_Z will be replaced by C_L and C_D:

$$\begin{aligned} C_X &= C_L \sin(\alpha) - C_D \cos(\alpha)\cos(\beta) \\ C_Z &= -C_L \cos(\alpha) - C_D \sin(\alpha)\cos(\beta). \end{aligned} \tag{1.27}$$

The nondimensional coefficients are highly nonlinear functions of present and past values of airspeed, angles of incidence of the air-relative velocity with respect to the aircraft body, aircraft rigid-body rotation rates, air-relative linear and angular accelerations, control surface deflections, and other nondimensional quantities. Based on CFD results, the nondimensional coefficients can be written as

$$C_L = C_{L0} + \Delta C_{L\alpha} + \Delta C_{L\beta} + \Delta C_{L\delta_e^i} + \Delta C_{L\delta_e^o} + \Delta C_{L\delta_e^c} + \Delta C_{L\delta_r} + \Delta C_{L\delta_a^i} + \Delta C_{L\delta_a^o}, \tag{1.28}$$

$$C_D = C_{D0} + \Delta C_{D\alpha} + \Delta C_{D\beta} + \Delta C_{D\delta_e^i} + \Delta C_{D\delta_e^o} + \Delta C_{D\delta_e^c} + \Delta C_{D\delta_r} + \Delta C_{D\delta_a^i} + \Delta C_{D\delta_a^o}, \tag{1.29}$$

$$C_Y = \Delta C_{Y\beta} + \Delta C_{Y\delta_e^i} + \Delta C_{Y\delta_e^o} + \Delta C_{Y\delta_e^c} + \Delta C_{Y\delta_r} + \Delta C_{Y\delta_a^i} + \Delta C_{Y\delta_a^o}. \tag{1.30}$$

The terms in C_L are

$$\begin{aligned} C_{L0} &= C_L\big|_{\alpha=0} & \Delta C_{L\alpha} &= C_L(\alpha) - C_L\big|_{\alpha=0} & \Delta C_{L\beta} &= C_L\big|_{\beta} - C_L\big|_{\beta=0} \\ \Delta C_{L\delta_e^i} &= C_L\big|_{\delta_e^i} - C_L\big|_{\delta_e^i=0} & \Delta C_{L\delta_e^o} &= C_L\big|_{\delta_e^o} - C_L\big|_{\delta_e^o=0} & \Delta C_{L\delta_e^c} &= C_L\big|_{\delta_e^c} - C_L\big|_{\delta_e^c=0} \\ \Delta C_{L\delta_r} &= C_L\big|_{\delta_r} - C_L\big|_{\delta_r=0} & \Delta C_{L\delta_a^i} &= C_L\big|_{\delta_a^i} - C_L\big|_{\delta_a^i=0} & \Delta C_{L\delta_a^o} &= C_L\big|_{\delta_a^o} - C_L\big|_{\delta_a^o=0}. \end{aligned} \tag{1.31}$$

The terms in C_D are

$$\begin{aligned}
C_{D0} &= C_D\big|_{\alpha=0} & \Delta C_{D\alpha} &= C_D(\alpha) - C_D\big|_{\alpha=0} & \Delta C_{D\beta} &= C_D\big|_{\beta} - C_D\big|_{\beta=0} \\
\Delta C_{D\delta_e^i} &= C_D\big|_{\delta_e^i} - C_D\big|_{\delta_e^i=0} & \Delta C_{D\delta_e^o} &= C_D\big|_{\delta_e^o} - C_D\big|_{\delta_e^o=0} & \Delta C_{D\delta_e^c} &= C_D\big|_{\delta_e^c} - C_D\big|_{\delta_e^c=0} \\
\Delta C_{D\delta_r} &= C_D\big|_{\delta_r} - C_D\big|_{\delta_r=0} & \Delta C_{D\delta_a^i} &= C_D\big|_{\delta_a^i} - C_D\big|_{\delta_a^i=0} & \Delta C_{D\delta_a^o} &= C_D\big|_{\delta_a^o} - C_D\big|_{\delta_a^o=0}.
\end{aligned} \tag{1.32}$$

The terms in C_Y are

$$\begin{aligned}
\Delta C_{Y\beta} &= C_Y\big|_{\beta} - C_Y\big|_{\beta=0} \\
\Delta C_{Y\delta_e^i} &= C_Y\big|_{\delta_e^i,\beta} - C_Y\big|_{\delta_e^i=0,\beta} - C_Y\big|_{\delta_e^i,\beta=0} + C_Y\big|_{\delta_e^i=0,\beta=0} \\
\Delta C_{Y\delta_e^o} &= C_Y\big|_{\delta_e^o,\beta} - C_Y\big|_{\delta_e^o=0,\beta} - C_Y\big|_{\delta_e^o,\beta=0} + C_Y\big|_{\delta_e^o=0,\beta=0} \\
\Delta C_{Y\delta_e^c} &= C_Y\big|_{\delta_e^c,\beta} - C_Y\big|_{\delta_e^c=0,\beta} - C_Y\big|_{\delta_e^c,\beta=0} + C_Y\big|_{\delta_e^c=0,\beta=0} \\
\Delta C_{Y\delta_r} &= C_Y\big|_{\delta_r} - C_Y\big|_{\delta_r=0} \quad \Delta C_{Y\delta_a^i} = C_Y\big|_{\delta_a^i} - C_Y\big|_{\delta_a^i=0} \quad \Delta C_{Y\delta_a^o} = C_Y\big|_{\delta_a^o} - C_Y\big|_{\delta_a^o=0}
\end{aligned} \tag{1.33}$$

Strictly speaking, the coefficients should be functions of angle of attack, angle of sideslip, true airspeed and altitude, etc. That is to say, the expression above should actually be, for example,

$$\Delta C_{L\delta_e^c} = \left(C_L\big|_{\delta_e^c} - C_L\big|_{\delta_e^c=0}\right)_{\alpha,\beta,|\boldsymbol{V}|,h}. \tag{1.34}$$

But for V24, **it is assumed that:**

- Airspeed during flight will be in the range of $20m/s < |\boldsymbol{V}| < 35m/s$ (Mach 0.06 - 0.1), within which the aerodynamic coefficients do not significantly change. (**Need validation, especially for airspeed as low as** $20m/s$).
- The altitude will not exceeds $500m$, so air pressure and air density can be approximated as constant.
- V24 will not conduct any maneuver with $\alpha > 30°$.

Based on those assumptions, the expression can be simplified to $\Delta C_{L\delta_e^c} = \left(C_L\big|_{\delta_e^c} - C_L\big|_{\delta_e^c=0}\right)_{\alpha,\beta}$. And for further simplification, the subscript α, β is also dropped.

The above model is in the form of a database developed by using interpolation, which means there is no explicit algebraic expression for all the nondimensional coefficients. For the use of flight control, linearization, either numerical or algebraical, can be applied to generate the linear model below:

$$C_L = C_{L0} + C_{L\alpha}\cdot\alpha + C_{L\beta}\cdot|\beta| + C_{L\delta_e^i}\cdot\delta_e^i + C_{L\delta_e^o}\cdot\delta_e^o + C_{L\delta_e^c}\cdot\delta_e^c + C_{L\delta_r}\cdot\delta_r + C_{L\delta_a^i}\cdot\delta_a^i + C_{L\delta_a^o}\cdot\delta_a^o \tag{1.35}$$

$$C_D = C_{D0} + C_{D\alpha}\cdot\alpha + C_{D\beta}\cdot|\beta| + C_{D\delta_e^i}\cdot\delta_e^i + C_{D\delta_e^o}\cdot\delta_e^o + C_{D\delta_e^c}\cdot\delta_e^c + C_{D\delta_r}\cdot\delta_r + C_{D\delta_a^i}\cdot\delta_a^i + C_{D\delta_a^o}\cdot\delta_a^o \tag{1.36}$$

$$C_Y = C_{Y\beta}\cdot|\beta| + C_{Y\delta_e^i}\cdot\delta_e^i + C_{Y\delta_e^o}\cdot\delta_e^o + C_{Y\delta_e^c}\cdot\delta_e^c + C_{Y\delta_r}\cdot\delta_r + C_{Y\delta_a^i}\cdot\delta_a^i + C_{Y\delta_a^o}\cdot\delta_a^o \tag{1.37}$$

Aerodynamic Moment

Assume that the aerodynamic moments acting on V24 resolved in body frame can be written in the form of

$$\boldsymbol{M_A}\Big|_{\mathcal{B}} = \bar{q}S \begin{bmatrix} bC_l \\ \bar{c}C_m \\ bC_n \end{bmatrix} \tag{1.38}$$

where b is the wing span, $\bar{c}$ is the mean aerodynamic chord of the wing and C_l, C_m, C_n are nondimensional coefficients of roll, pitch and yaw aerodynamic moments. For V24, the above parameters are defined as in Figure.1.4 and the corresponsding values are listed below:

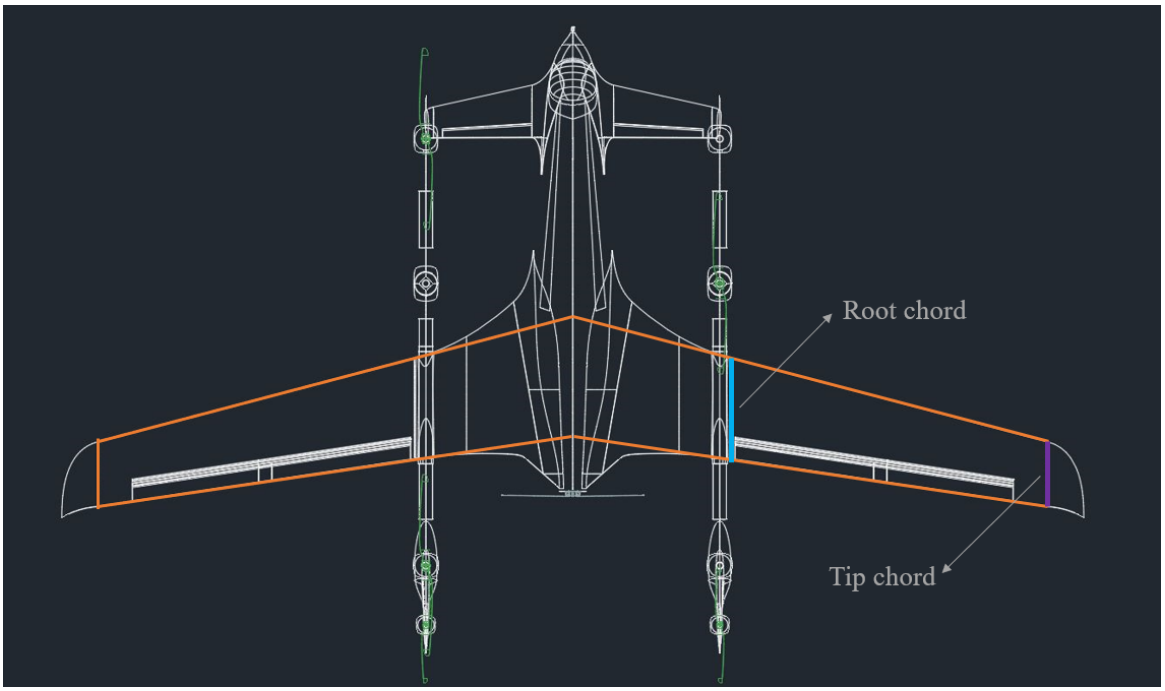

(a) Wing reference area used for V24 (area enclosed by orange lines) and definition of root chord and tip chord.

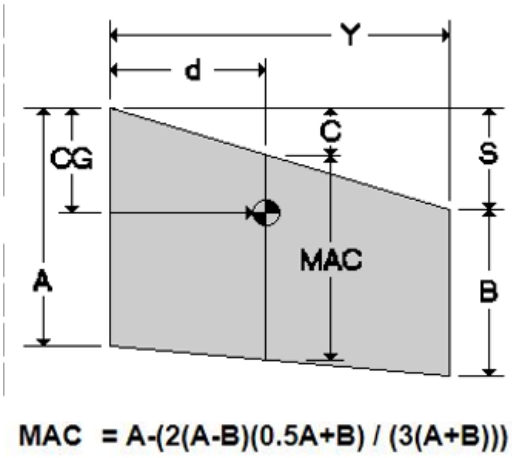

(b) Method used to compute mean aerodynamic chord.

Figure 1.4: Wing reference area and mean aerodynamic chord.

- wing span (b): 4.2 m,
- wing reference area (S): 1.3573 m^2,
- mean aerodynamic chord ($\bar{c}$): 0.3523 m.

Based on CFD results, the nondimensional coefficients can be written as

$$\begin{aligned} C_l = \Delta C_{l\beta} + \Delta C_{l\delta_e^i} + \Delta C_{l\delta_e^o} + \Delta C_{l\delta_e^c} + \Delta C_{l\delta_r} + \Delta C_{l\delta_a^i} + \Delta C_{l\delta_e^o} \\ + \frac{b}{2|\boldsymbol{V}|}(C_{lp} \cdot p + C_{lr} \cdot r) \end{aligned} \tag{1.39}$$

$$\begin{aligned} C_m = C_{m0} + \Delta C_{m\alpha} + \Delta C_{m\beta} + \Delta C_{m\delta_e^i} + \Delta C_{m\delta_e^o} + \Delta C_{m\delta_e^c} + \Delta C_{m\delta_r} + \Delta C_{m\delta_a^i} \\ + \Delta C_{m\delta_a^o} + \frac{\bar{c}}{2|\boldsymbol{V}|} \cdot C_{mq} \cdot q + (-C_Z) \cdot \frac{-x_{CG,ref}}{100} \end{aligned} \tag{1.40}$$

$$\begin{aligned} C_n = \Delta C_{n\beta} + \Delta C_{n\delta_e^i} + \Delta C_{n\delta_e^o} + \Delta C_{n\delta_e^c} + \Delta C_{n\delta_r} + \Delta C_{n\delta_a^i} + \Delta C_{n\delta_e^o} \\ + \frac{b}{2|\boldsymbol{V}|}(C_{np} \cdot p + C_{nr} \cdot r) + C_Y(-x_{CG,ref})\frac{\bar{c}}{100b} \end{aligned} \tag{1.41}$$

where $x_{CG,ref}$ is the position of $c.g.$ used in CFD calculation. In other words, if the $c.g$ has been moved $0.03m$ towards rear, then $x_{CG,ref} = 0.03m$.

The terms in C_l are

$$\begin{aligned} \Delta C_{l\beta} &= C_l\big|_{\beta} - C_l\big|_{\beta=0} \\ \Delta C_{l\delta_e^i} &= C_l\big|_{\delta_e^i,\beta} - C_l\big|_{\delta_e^i=0,\beta} - C_l\big|_{\delta_e^i,\beta=0} + C_l\big|_{\delta_e^i=0,\beta=0} \\ \Delta C_{l\delta_e^o} &= C_l\big|_{\delta_e^o,\beta} - C_l\big|_{\delta_e^o=0,\beta} - C_l\big|_{\delta_e^o,\beta=0} + C_l\big|_{\delta_e^o=0,\beta=0} \\ \Delta C_{l\delta_e^c} &= C_l\big|_{\delta_e^c,\beta} - C_l\big|_{\delta_e^c=0,\beta} - C_l\big|_{\delta_e^c,\beta=0} + C_l\big|_{\delta_e^c=0,\beta=0} \\ \Delta C_{l\delta_r} &= C_l\big|_{\delta_r} - C_l\big|_{\delta_r=0} \quad \Delta C_{l\delta_a^i} = C_l\big|_{\delta_a^i} - C_l\big|_{\delta_a^i=0} \quad \Delta C_{l\delta_a^o} = C_l\big|_{\delta_a^o} - C_l\big|_{\delta_a^o=0} \end{aligned} \tag{1.42}$$

The terms in C_m are

$$\begin{aligned} C_{m0} &= C_m\big|_{\alpha=0} & \Delta C_{m\alpha} &= C_m(\alpha) - C_m\big|_{\alpha=0} & \Delta C_{m\beta} &= C_m\big|_{\beta} - C_m\big|_{\beta=0} \\ \Delta C_{m\delta_e^i} &= C_m\big|_{\delta_e^i} - C_m\big|_{\delta_e^i=0} & \Delta C_{m\delta_e^o} &= C_m\big|_{\delta_e^o} - C_m\big|_{\delta_e^o=0} & \Delta C_{m\delta_e^c} &= C_m\big|_{\delta_e^c} - C_m\big|_{\delta_e^c=0} \\ \Delta C_{m\delta_r} &= C_m\big|_{\delta_r} - C_m\big|_{\delta_r=0} & \Delta C_{m\delta_a^i} &= C_m\big|_{\delta_a^i} - C_m\big|_{\delta_a^i=0} & \Delta C_{m\delta_a^o} &= C_m\big|_{\delta_a^o} - C_m\big|_{\delta_a^o=0}. \end{aligned} \tag{1.43}$$

The terms in C_n are

$$\begin{aligned} \Delta C_{n\beta} &= C_n\big|_{\beta} - C_n\big|_{\beta=0} \\ \Delta C_{n\delta_e^i} &= C_n\big|_{\delta_e^i,\beta} - C_n\big|_{\delta_e^i=0,\beta} - C_n\big|_{\delta_e^i,\beta=0} + C_n\big|_{\delta_e^i=0,\beta=0} \\ \Delta C_{n\delta_e^o} &= C_n\big|_{\delta_e^o,\beta} - C_n\big|_{\delta_e^o=0,\beta} - C_n\big|_{\delta_e^o,\beta=0} + C_n\big|_{\delta_e^o=0,\beta=0} \\ \Delta C_{n\delta_e^c} &= C_n\big|_{\delta_e^c,\beta} - C_n\big|_{\delta_e^c=0,\beta} - C_n\big|_{\delta_e^c,\beta=0} + C_n\big|_{\delta_e^c=0,\beta=0} \\ \Delta C_{n\delta_r} &= C_n\big|_{\delta_r} - C_n\big|_{\delta_r=0} \quad \Delta C_{n\delta_a^i} = C_n\big|_{\delta_a^i} - C_n\big|_{\delta_a^i=0} \quad \Delta C_{n\delta_a^o} = C_n\big|_{\delta_a^o} - C_n\big|_{\delta_a^o=0} \end{aligned} \tag{1.44}$$

To simplify the nonlinear relation, as in the previous section, a linear aerodynamic model under small perturbation for quasi-steady flow at low mach number will be considered. The nondimensional coefficients are written as

$$C_l = C_{l\beta}\cdot|\beta| + C_{l\delta_e^i}\cdot\delta_e^i + C_{l\delta_e^o}\cdot\delta_e^o + C_{l\delta_e^c}\cdot\delta_e^c + C_{l\delta_r}\cdot\delta_r + C_{l\delta_a^i}\cdot\delta_a^i + C_{l\delta_a^o}\cdot\delta_a^o + \frac{b}{2|\boldsymbol{V}|}(C_{lp}\cdot p + C_{lr}\cdot r) \quad (1.45)$$

$$C_m = C_{m0} + C_{m\alpha}\cdot\alpha + C_{m\beta}\cdot|\beta| + C_{m\delta_e^i}\cdot\delta_e^i + C_{m\delta_e^o}\cdot\delta_e^o + C_{m\delta_e^c}\cdot\delta_e^c + C_{m\delta_r}\cdot\delta_r + C_{m\delta_a^i}\cdot\delta_a^i + C_{m\delta_a^o}\cdot\delta_a^o + \frac{\bar{c}}{2|\boldsymbol{V}|}\cdot C_{mq}\cdot q + (-C_Z)\cdot\frac{-x_{CG,ref}}{100} \quad (1.46)$$

$$C_n = C_{n\beta}\cdot|\beta| + C_{n\delta_e^i}\cdot\delta_e^i + C_{n\delta_e^o}\cdot\delta_e^o + C_{n\delta_e^c}\cdot\delta_e^c + C_{n\delta_r}\cdot\delta_r + C_{n\delta_a^i}\cdot\delta_a^i + C_{n\delta_a^o}\cdot\delta_a^o + \frac{b}{2|\boldsymbol{V}|}(C_{np}\cdot p + C_{nr}\cdot r) + C_Y(-x_{CG,ref})\frac{\bar{c}}{100b} \quad (1.47)$$

$\lvert\boldsymbol{V}\rvert[m/s]$	35
$\alpha[^\circ]$	$-10,-8,-6,-4,-2,0,2,4,6,8,10,12,15,17,20,22,25$
$\beta[^\circ]$	$-20,-15,-10,-5,0,5,10,15,20$
$\delta_a^i[^\circ]$	$0,5,10,15,20,25,30$
$\delta_a^o[^\circ]$	$0,5,10,15,20,25,30$
$\delta_a^c[^\circ]$	$0,5,10,15,20,25,30$
$\delta_e^i[^\circ]$	$-30,-25,-20,-15,-10,-5,0,5,10,15,20,25,30$
$\delta_e^o[^\circ]$	$-30,-25,-20,-15,-10,-5,0,5,10,15,20,25,30$
$\delta_e^c[^\circ]$	$-30,-25,-20,-15,-10,-5,0,5,10,15,20,25,30$
$\delta_r[^\circ]$	$-30,-25,-20,-15,-10,-5,0,5,10,15,20,25,30$

Table 1.1: Data points at which CFD was used. The data base is formed by using Hermite interpolation on those data points.

It it worth noting that all three pairs of control surfaces can be used as elevons (one pair on canards and two on main wings), while the current flight controller assign one pair of control surfaces only one single function. This elevon property can be observed in Eq.1.40 where C_m is not only a function of canard deflection but also a function of deflection of control surfaces on main wings.

1.5.3 Combined Dynamic Model

The combined dynamic model is obtained by plugging Eq.**??**, Eq.1.25 and Eq.1.24 into Eq.1.12.

Chapter 2

INDI Controller Design

2.1 Controller Architecture

Euler's equation of motion(Eq.1.12) can be rewritten as

$$\dot{\boldsymbol{\Omega}} = \boldsymbol{I}_v^{-1}\boldsymbol{M_v} - \boldsymbol{I}_v^{-1}\boldsymbol{\Omega} \times \boldsymbol{I}_v\boldsymbol{\Omega} \tag{2.1}$$

where $\boldsymbol{M_v}$ will be acting as the control input. As presented in Chapter.1, $\boldsymbol{M_v}$ is a highly nonlinear function and hence a process of linearization and simplification must be conducnted before the algorithm of incremental nonlinear dynamic inverse(INDI) can be applied.

2.1.1 Simplification

This section lists the simplifications used in developing INDI controller. Some of these simplifications will be eliminated in the future.

- The INDI controller will only be used in fixed-wing flight.
- The dynamic models of all actuators are ignored, which means the reponses are all instantaneous.
- None of the control surfaces can be used as elevon — namely, the canard will only be used as elevator and control surfaces on the main wings will only be used as ailerons. Furthermore, the two control surfaces on the same side (surface 3,4 and 5,6) will be considered as one single control surface. In other words,

$$\delta_e^i = \delta_e^o = 0, \qquad \delta_a^i = \delta_a^o. \tag{2.2}$$

- The position of *c.g.* is the same as that used in CFD calculation. That is,

$$x_{CG,ref} = 0. \tag{2.3}$$

2.1.2 INDI Angular Rate Control

The architecture of INDI angular rate control is shown in Figure.2.1. There are three important parts that need careful design and consideration, namely, the outer loop controller, the INDI inner loop, and the angular acceleration estimator.

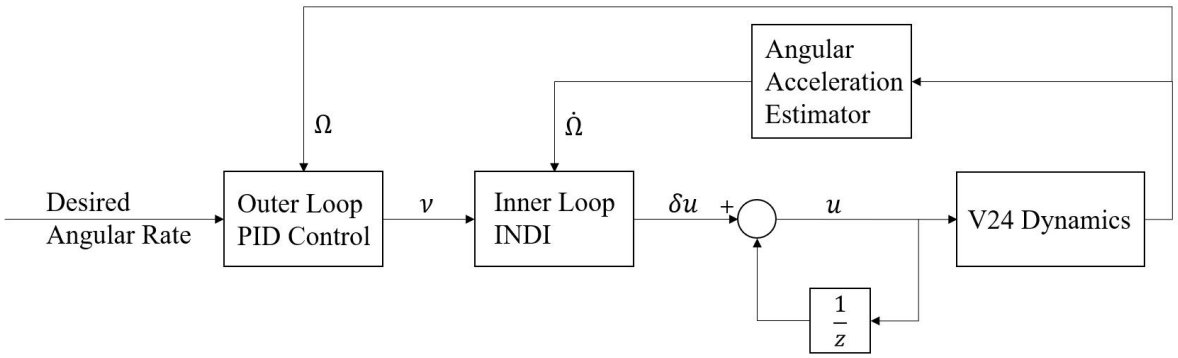

Figure 2.1: INDI Controller architecture of angular acceleration. $\boldsymbol{\Omega}$ is the angular rate measurement obtained from the states estimator(a EKF for V24).

INDI

Let $\boldsymbol{x} = [\boldsymbol{x}_1] = [p, q, r]^T$ be one state vector. Based on the simplification in Sec.2.1.1, define the vector of control inputs, u, as

$$\boldsymbol{u} = \begin{bmatrix} \delta_a \\ \delta_e \\ \delta_r \end{bmatrix} = \begin{bmatrix} \delta_a^i \\ \delta_e^c \\ \delta_r \end{bmatrix} = \begin{bmatrix} \delta_a^o \\ \delta_e^c \\ \delta_r \end{bmatrix}. \tag{2.4}$$

Let $\boldsymbol{x}_0 = [p_0, q_0, r_0]^T$ and $\boldsymbol{u}_0 = [\delta_{a0}, \delta_{e0}, \delta_{r0}]$ be an operating point. Taking a Taylor series expansion for Eq.2.1 around a nominal operating point $(\boldsymbol{x}_0, \boldsymbol{u}_0)$ and drop the higher order terms:

$$\begin{aligned} \dot{\boldsymbol{\Omega}} \approx \boldsymbol{I}_v^{-1}\boldsymbol{M_v}(\boldsymbol{x}_0, \boldsymbol{u}_0) - \boldsymbol{I}_v^{-1}\boldsymbol{\Omega}(\boldsymbol{x}_0, \boldsymbol{u}_0) \times \boldsymbol{I}_v\boldsymbol{\Omega}(\boldsymbol{x}_0, \boldsymbol{u}_0) + \boldsymbol{I}_v^{-1}\frac{\partial \boldsymbol{M_v}(\boldsymbol{x}, \boldsymbol{u})}{\partial \boldsymbol{x}}(\boldsymbol{x} - \boldsymbol{x}_0) \\ + \boldsymbol{I}_v^{-1}\frac{\partial \boldsymbol{M_v}(\boldsymbol{x}, \boldsymbol{u})}{\partial \boldsymbol{u}}(\boldsymbol{u} - \boldsymbol{u}_0) + \boldsymbol{I}_v^{-1}\frac{\partial [\boldsymbol{\Omega}(\boldsymbol{x}) \times \boldsymbol{I}_v\boldsymbol{\Omega}(\boldsymbol{x})]}{\partial \boldsymbol{x}}(\boldsymbol{x} - \boldsymbol{x}_0) \end{aligned} \tag{2.5}$$

By inspecting that $\boldsymbol{I}_v^{-1}\boldsymbol{M_v}(x_0, u_0) - \boldsymbol{I}_v^{-1}\boldsymbol{\Omega}(x_0, u_0) \times \boldsymbol{I}_v\boldsymbol{\Omega}(x_0, u_0) = \dot{\boldsymbol{\Omega}}_0$, and applying the principle of timescale separation, Eq.2.6 can be reduced to

$$\dot{\boldsymbol{\Omega}} \approx \dot{\boldsymbol{\Omega}}_0 + \boldsymbol{I}_v^{-1}\frac{\partial \boldsymbol{M_v}(\boldsymbol{x}, \boldsymbol{u})}{\partial \boldsymbol{u}}(\boldsymbol{u} - \boldsymbol{u}_0). \tag{2.6}$$

According to the assumption that multicopter is completely shut off during fixed-wing flight, $\boldsymbol{M_v}$ now refduces to

$$\begin{aligned} \boldsymbol{M_v} &= \boldsymbol{M_A} + \boldsymbol{M_r} = \boldsymbol{M_A} - \boldsymbol{M_{rg}} = \boldsymbol{M_A} - \boldsymbol{M_p} \\ &= \bar{q}S \begin{bmatrix} bC_l \\ \bar{c}C_m \\ bC_n \end{bmatrix} - \begin{bmatrix} I_{p_{xx}}\dot{\boldsymbol{\omega}}_{px} + \tau_p \\ rI_{p_{xx}}\boldsymbol{\omega}_{px} \\ -qI_{p_{xx}}\boldsymbol{\omega}_{px} \end{bmatrix} \end{aligned} \tag{2.7}$$

Based on simplifications in Sec.2.1.1, the linearized aerodynamic model in Eq.1.45-1.47 now reduces to

$$C_l = C_{l\beta} \cdot |\beta| + C_{l\delta_e^c} \cdot \delta_e^c + C_{l\delta_r} \cdot \delta_r + (C_{l\delta_a^i} + C_{l\delta_a^o})\delta_a + \frac{b}{2|\boldsymbol{V}|}(C_{lp} \cdot p + C_{lr} \cdot r) \tag{2.8}$$

$$C_m = C_{m0} + C_{m\alpha} \cdot \alpha + C_{m\beta} \cdot |\beta| + C_{m\delta_e^c} \cdot \delta_e^c + C_{m\delta_r} \cdot \delta_r + (C_{m\delta_a^i} + C_{m\delta_a^o})\delta_a + \frac{\bar{c}}{2|\boldsymbol{V}|} \cdot C_{mq} \cdot q \quad (2.9)$$

$$C_n = C_{n\beta} \cdot |\beta| + C_{n\delta_e^c} \cdot \delta_e^c + C_{n\delta_r} \cdot \delta_r + (C_{n\delta_a^i} + C_{n\delta_a^o})\delta_a + \frac{b}{2|\boldsymbol{V}|}(C_{np} \cdot p + C_{nr} \cdot r) \quad (2.10)$$

Then it can be shown that

$$\frac{\partial \boldsymbol{M_v}(\boldsymbol{x}, \boldsymbol{u})}{\partial \boldsymbol{u}} = \bar{q}S \begin{bmatrix} b(C_{l\delta_a^i} + C_{l\delta_a^o}) & bC_{l\delta_e^c} & bC_{l\delta_r} \\ \bar{c}(C_{m\delta_a^i} + C_{m\delta_a^o}) & \bar{c}C_{m\delta_e^c} & \bar{c}C_{m\delta_r} \\ b(C_{n\delta_a^i} + C_{n\delta_a^o}) & bC_{n\delta_e^c} & bC_{n\delta_r} \end{bmatrix} = \boldsymbol{B} \quad (2.11)$$

Let $\boldsymbol{\delta u} = \boldsymbol{u} - \boldsymbol{u}_0 = [\delta_a - \delta_{a0}, \delta_e - \delta_{e0}, \delta_r - \delta_{r0}]^T$, then Eq.2.6 becomes

$$\dot{\boldsymbol{\Omega}} \approx \dot{\boldsymbol{\Omega}}_0 + \boldsymbol{I}_v^{-1}\boldsymbol{B}\boldsymbol{\delta u}. \quad (2.12)$$

Replacing the angular acceleration($\dot{\boldsymbol{\Omega}}$) by the pseudo control input($\boldsymbol{\nu}$) from the outter loop and inverting Eq.2.12:

$$\boldsymbol{\delta u} = \boldsymbol{B}^{-1}\boldsymbol{I}_v(\boldsymbol{\nu} - \boldsymbol{\Omega}) \quad (2.13)$$

Outer Loop

The outer loop uses an nonlinear dynamic inversion(NDI) controller.

Angular Acceleration Estimator

As shown in Figure.2.2, a complementary filter is used to estimate the angular acceleration of the airframe. The predicted angular acceleration can be obtained by solving Eq.1.14 with $\dot{p}, \dot{q}$

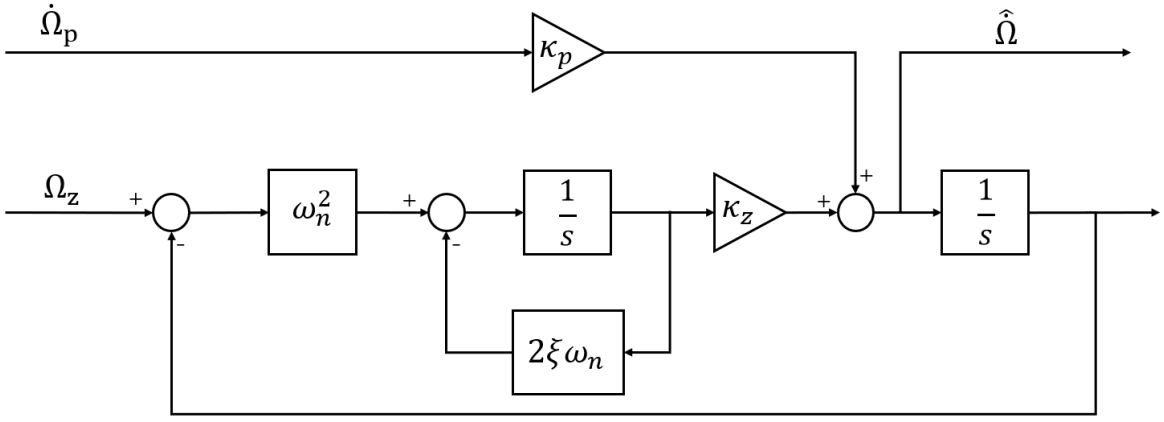

Figure 2.2: The complementary filter used to estimate the angular acceleration of the airframe. $\dot{\boldsymbol{\Omega}}_p$ is the predicted angular acceleration using aircraft dynamic model, $\boldsymbol{\Omega}_z$ is the measured angular rate output from the state estimator(a EKF for V24), $\hat{\dot{\boldsymbol{\Omega}}}$ is the estimated angular acceleration, κ_p and κ_z are gains for predicted and measured angular acceleration, ω_n and ξ are the natural frequency and damping ratio of the second order filter.

and $\dot{r}$ as unknowns.

$$\begin{aligned} \dot{p} &= \frac{I_{xz}}{I_x I_z - I_{xz}^2}\left[\frac{I_z}{I_{xz}}M_{vx} + M_{vz} + pqI_z - qrI_{xz} - \frac{I_z}{I_{xz}} - \frac{I_z}{I_{xz}}(I_z - I_y)qr - pq(I_y - I_x)\right] \\ \dot{q} &= \frac{M_{vy}}{I_y} - \frac{pr(I_x - I_z) - (p^2 - r^2)I_{xz}}{I_y} \end{aligned} \quad (2.14)$$

Appendices

Appendix A

Experimental Determination of Moment of Inertia

Appendix B

Calculation of Propeller Lift and Torque

RPM	VZ(m/s)	Lift(N)	Drag(N)	MZ(Nm)	MX(Nm)	MY(Nm)	Lift(Kg)
3000	10	5.188	2.877	-0.842	0.000	0.000	0.529
3500	10	14.372	4.627	-1.299	0.000	0.000	1.467
4000	10	26.256	6.753	-1.849	0.000	0.000	2.679
4500	10	41.060	9.311	-2.501	0.000	0.000	4.190
3000	7.5	14.276	3.772	-1.030	0.000	0.000	1.457
3500	7.5	25.359	5.647	-1.503	0.000	0.000	2.588
4000	7.5	39.190	7.894	-2.063	0.000	0.000	3.999
4500	7.5	55.895	10.549	-2.723	0.000	0.000	5.704
3000	5.0	23.971	4.617	-1.184	0.000	0.000	2.446
3500	5.0	36.839	6.584	-1.666	0.000	0.000	3.759
4000	5.0	52.466	8.914	-2.237	0.000	0.000	5.354
4500	5.0	71.010	11.644	-2.907	0.000	0.000	7.246
3000	2.5	33.848	5.297	-1.294	0.000	0.000	3.454
3500	2.5	48.425	7.324	-1.782	0.000	0.000	4.941
4000	2.5	65.798	9.719	-2.361	0.000	0.000	6.714
4500	2.5	86.127	12.520	-3.040	0.000	0.000	8.788
3000	0.0	43.539	5.721	-1.348	0.000	0.000	4.443
3500	0.0	59.753	7.789	-1.839	0.000	0.000	6.097
4000	0.0	78.806	10.231	-2.422	0.000	0.000	8.041
4500	0.0	100.865	13.082	-3.107	0.000	0.000	10.292
3000	-2.5	52.548	5.820	-1.341	0.000	0.000	5.362
3500	-2.5	70.348	7.922	-1.834	0.000	0.000	7.178
4000	-2.5	91.017	10.402	-2.420	0.000	0.000	9.287
4500	-2.5	114.740	13.296	-3.110	0.000	0.000	11.708
3000	-5.0	60.275	5.634	-1.283	0.000	0.000	6.150
3500	-5.0	79.670	7.738	-1.775	0.000	0.000	8.130
4000	-5.0	101.946	10.250	-2.362	0.000	0.000	10.403
4500	-5.0	127.301	13.174	-3.054	0.000	0.000	12.990
3000	-7.5	66.170	5.292	-1.194	0.000	0.000	6.752
3500	-7.5	87.140	7.386	-1.679	0.000	0.000	8.892
4000	-7.5	111.008	9.885	-2.262	0.000	0.000	11.327
4500	-7.5	137.965	12.807	-2.953	0.000	0.000	14.078
3000	-10	69.894	4.878	-1.094	0.000	0.000	7.132
3500	-10	92.396	6.900	-1.562	0.000	0.000	9.428
4000	-10	117.801	9.375	-2.135	0.000	0.000	12.020
4500	-10	146.347	12.271	-2.817	0.000	0.000	14.933

Table B.1: Influence of vertical movement on torque and lift of propeller 6. VZ is the speed of vertical movement: VZ = $V_z^{\mathcal{B}}$. MX, MY and MZ are moments acting on V24 airframe along the three axes of body frame.

RPM	VX(m/s)	Lift(N)	Drag(N)	MZ(Nm)	MX(Nm)	MY(Nm)	Lift(Kg)
3000	10	44.088	5.809	-1.362	1.418	0.000	4.499
3500	10	60.319	7.881	-1.854	1.682	0.000	6.155
4000	10	79.393	10.327	-2.439	1.961	0.000	8.101
4500	10	101.478	13.185	-3.126	2.258	0.000	10.355
3000	7.5	43.848	5.771	-1.356	1.063	0.000	4.474
3500	7.5	60.072	7.841	-1.847	1.262	0.000	6.130
4000	7.5	79.136	10.285	-2.431	1.470	0.000	8.075
4500	7.5	101.210	13.140	-3.117	1.693	0.000	10.328
3000	5.0	43.676	5.743	-1.351	0.709	0.000	4.457
3500	5.0	59.895	7.812	-1.843	0.841	0.000	6.112
4000	5.0	78.953	10.255	-2.426	0.980	0.000	8.056
4500	5.0	101.018	13.108	-3.112	1.129	0.000	10.308
3000	2.5	43.573	5.726	-1.348	0.354	0.000	4.446
3500	2.5	59.788	7.795	-1.840	0.420	0.000	6.101
4000	2.5	78.843	10.237	-2.423	0.490	0.000	8.045
4500	2.5	100.903	13.088	-3.108	0.564	0.000	10.296
3000	0.0	43.539	5.721	-1.348	0.000	0.000	4.443
3500	0.0	59.753	7.789	-1.839	0.000	0.000	6.097
4000	0.0	78.806	10.231	-2.422	0.000	0.000	8.041
4500	0.0	100.865	13.082	-3.107	0.000	0.000	10.292
3000	-2.5	43.573	5.726	-1.348	-0.354	0.000	4.446
3500	-2.5	59.788	7.795	-1.840	-0.420	0.000	6.101
4000	-2.5	78.843	10.237	-2.423	-0.490	0.000	8.045
4500	-2.5	100.903	13.088	-3.108	-0.564	0.000	10.296
3000	-5.0	43.676	5.743	-1.351	-0.709	0.000	4.457
3500	-5.0	59.895	7.812	-1.843	-0.841	0.000	6.112
4000	-5.0	78.953	10.255	-2.426	-0.980	0.000	8.056
4500	-5.0	101.018	13.108	-3.112	-1.129	0.000	10.308
3000	-7.5	43.848	5.771	-1.356	-1.063	0.000	4.474
3500	-7.5	60.072	7.841	-1.847	-1.262	0.000	6.130
4000	-7.5	79.136	10.285	-2.431	-1.470	0.000	8.075
4500	-7.5	101.210	13.210	-3.117	-1.693	0.000	10.328
3000	-10	44.088	5.809	-1.362	-1.418	0.000	4.499
3500	-10	60.319	7.881	-1.854	-1.682	0.000	6.155
4000	-10	79.393	10.327	-2.439	-1.961	0.000	8.101
4500	-10	101.478	13.185	-3.126	-2.258	0.000	10.355

Table B.2: Influence of horizontal movement on torque and lift of propeller 6. VX is the speed of vertical movement: VX = $V_x^{\mathcal{B}}$. MX, MY and MZ are moments acting on V24 airframe along the three axes of body frame.

Bibliography

[1] Vladislav Klein, Eugene A. Morelli. *Aircraft System Identification: Theory and Practice.* American Institute of Aeronautics and Astronautics, Inc., 2006, ISBN 1-56347-832-3.

[2] Ewoud J. J. Smeur, Qiping Chu, Guido C. H. E. de Croon. *Adaptive Incremental Nonlinear Dynamic Inversion for Attitude Control of Micro Air Vehicles.* JOURNAL OF GUIDANCE, CONTROL, AND DYNAMICS, Vol. 39, No. 3, March 2016

[3] Gabriel M. Hoffmann, Haomiao Huang, Steven L. Waslander, Claire J. Tomlin. *Quadrotor Helicopter Flight Dynamics and Control: Theory and Experiment.*

[4] Limin Wu, Yijie Ke and Ben M. Chen. *Systematic Modeling of Rotor Dynamics for Small Unmanned Aerial Vehicles.*